EMRinger: side chain–directed model and map validation for 3D cryo-electron microscopy

Benjamin A Barad[1,2], Nathaniel Echols[3],
Ray Yu-Ruei Wang[4,5], Yifan Cheng[6], Frank DiMaio[5,7],
Paul D Adams[3,8] & James S Fraser[1]

Advances in high-resolution cryo-electron microscopy (cryo-EM) require the development of validation metrics to independently assess map quality and model geometry. We report EMRinger, a tool that assesses the precise fitting of an atomic model into the map during refinement and shows how radiation damage alters scattering from negatively charged amino acids. EMRinger (https://github.com/fraser-lab/EMRinger) will be useful for monitoring progress in resolving and modeling high-resolution features in cryo-EM.

Recent computational and experimental developments in single-particle cryo-EM now make it possible, in some cases, to build atomic models of proteins and protein assemblies without using any reference structures[1]. Because such structures are often inaccessible to X-ray crystallography or NMR[2], it is important to determine the reliability of the resulting atomic models, and in particular side chain placement, for their eventual use in directing detailed mechanistic studies or drug development[3].

Validation of all-atom *de novo* cryo-EM models presents several unique challenges[4]. First, the Coulomb potential map must be validated through assessment of the 'gold standard' Fourier shell correlation (FSC) between two independently refined half-maps[5]. The chemical reasonableness of the model must then be assessed with tools commonly applied in X-ray crystallography[6]. As in crystallography, it is essential to balance the agreement to experimental data with the deviation from ideal geometry while maintaining acceptable stereochemistry, Ramachandran statistics[7], side chain rotamers[8] and clash scores[6].

The weighting between data and prior structural knowledge is key to the third step of model-to-map validation: determining whether the structure is accurately fitted, but not over-fitted, to the map[9]. Several proposed cross-validation[9–11] can help to ensure that the model is not only reasonable but also well fitted to the map. However, simple correlation metrics tend to be dominated by low-resolution, high-signal features, which can render it difficult to assess the reliability of the highest-resolution features of EM maps, such as side chain or ligand conformations[11,12]. These problems can potentially be corrected through monitoring of the correlation in Fourier space at high frequency[9] or use of the real space correlation to band-pass–filtered maps as a cross-validation target for refinement[11].

An alternative solution for assessing the reliability of high-resolution models is to examine statistical signatures of the weaker, high-resolution data. Here, we extend Ringer, an approach that detects unmodeled alternative conformations in electron density maps generated by high-resolution X-ray crystallography[13,14], to directly reveal the side chain information content of EM maps. This approach, EMRinger (https://github.com/fraser-lab/EMRinger and **Supplementary Software**), interpolates the normalized value of the cryo-EM map at each potential position of the Cγ position around the χ1 dihedral angle, assuming the currently modeled N, Cα and Cβ atomic positions (**Fig. 1a**). We next plot the distribution of map values by dihedral angle (**Fig. 1b**), which reveals local information about both the map and correctness of the backbone of the atomic model. The peak in the distribution represents the most probable position of the Cγ atom of the side chain, even when it is not immediately obvious 'by eye'. The position of Cγ is constrained to avoid 'eclipsed' steric overlaps[15]. This bias is confirmed by high-resolution X-ray structures[8,16]. We therefore expected that high-quality EM maps with well-fit backbone models would be enriched in density peaks near the rotameric χ1 dihedral (N-Cα-Cβ-Cγ) angles of 60°, 180° and 300° (−60°)[17].

However, there are several reasons, including noise in the map or an inaccurate model, that a side chain peak might occur at a nonrotameric angle. For example, Gln519 of TrpV1 (ref. 18) (PDB 3J5P) is modeled in a rotameric position but has a peak at a nonrotameric angle in a 3.27-Å resolution map (EMDB 5778) (**Fig. 1a,b**). We observed singular peaks for most side chains in the TrpV1 map, which further suggests that noise is not the main reason that the peak occurs in a nonrotameric position. Alternatively, a peak in a nonrotameric position can indicate that the model is incorrect. If the N, Cα and Cβ atoms are positioned incorrectly in the strong potential surrounding the backbone, EMRinger will measure the map values in the wrong locations. It is important to note that this occurs even when the side chain is already modeled as rotameric. Changing the modeled side chain dihedral angle

Figure 1 | EMRinger χ_1 map value sampling reports on backbone position and guides side chain conformation. (**a**) The side chain of TrpV1 Gln519 of chain C (EMDB 5778, PDB 3J5P), fitted, with a real space correlation coefficient (RSCC) of 0.590, to the potential map, shown at an isolevel of 10. The side chain χ_1 angle is modeled at 168°. (**b**) The EMRinger scan, reflected by the pink ring in **a**, for Gln519 of chain C. The density peak, shown as a pink sphere in **a**, occurs at 130°. Rotameric regions of dihedral space are shown as gray bars. (**c**) Rotation of the side chain so that the χ_1 angle is at the map value peak (RSCC = 0.526). The side chain χ_1 is modeled at 130°. (**d**) The EMRinger scan for the modified side chain position. The density peak, shown as a pink sphere in **c**, occurs at 130°. (**e**) Correction of the backbone position with Rosetta refinement[19] to place the model near a χ_1 map value peak results in a small reduction on the overall correlation of the residue to the map (RSCC = 0.442). The side chain χ_1 angle is modeled at 178°. (**f**) The EMRinger scan for the modified backbone position. The density peak, shown as a pink sphere in **e**, occurs at 175°.

does not affect the result of EMRinger because the measurement relies only on the positions of the backbone and Cβ atoms (**Fig. 1c,d**). In contrast, a small backbone adjustment places the Cγ in the map value peak while maintaining a rotameric side chain model, excellent stereochemistry and a good map correlation (**Fig. 1e,f**).

To test the quality of model to map fit, we quantified the enrichment of EMRinger peaks in rotameric regions (within 30° of 60°, 180° or 300°) as a function of map value. We recorded the position and map value of the peak for each side chain χ_1 angle in the 3.2-Å resolution 20S proteasome map (EMDB 5623, PDB 3J9I) and observed that the distribution becomes more sharply peaked as the map value cutoff increases (**Fig. 2a** and **Supplementary Fig. 1a,b**). At lower cutoffs, noise flattened the results, with less enrichment for peaks in rotameric regions. Although rotameric regions are sampled more at higher cutoffs, fewer residues had local map value peaks above these cutoffs, and noise from counting statistics dominated (**Fig. 2b**). To quantify the relationship between sample size and rotameric enrichment, we used the normal approximation to the binomial distribution to generate a model-length independent validation statistic: the EMRinger score (**Fig. 2c** and **Supplementary Fig. 2**). For the 20S proteasome,
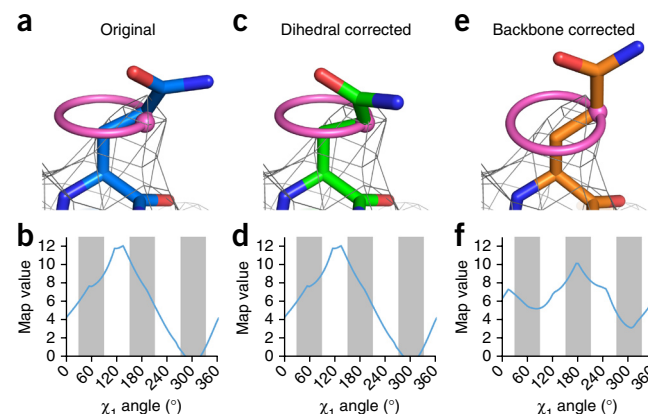
the EMRinger score was maximized at the 0.242 normalized map value cutoff, and the signal was dominated by 1,547 rotameric map value peaks, compared to 555 nonrotameric peaks (**Supplementary Fig. 3**). EMRinger scores are always calculated with a sampling angle of 5° to avoid inconsistent scoring and are for the most part independent of grid spacing changes owing to binning (**Supplementary Fig. 4b–d**).

We then sampled a series of cryo-EM maps deposited in the Electron Microscopy Data Bank (EMDB) spanning a resolution range of 3–5 Å, with atomic models built into the map density (**Fig. 2d** and **Supplementary Table 1**). Because a random distribution should produce an EMRinger score of 0, the trend suggests that the χ_1 angle of side chains can be resolved at 4.5-Å resolution or better. We observed similar trends in decreasing EMRinger score as maps of the T20S proteasome were progressively low-pass filtered (**Supplementary Fig. 4**). We observed a notable exception to the trend of increasing score with higher resolution in TrpV1 (ref. 18) (**Fig. 2d**), which had a low EMRinger score (0.56) despite its high-resolution map (3.27 Å). This *de novo* model was built manually and not subject to real- or reciprocal-space refinement. When we excluded the poorly resolved ankyrin domain of TrpV1, the EMRinger score increased to 1.17,
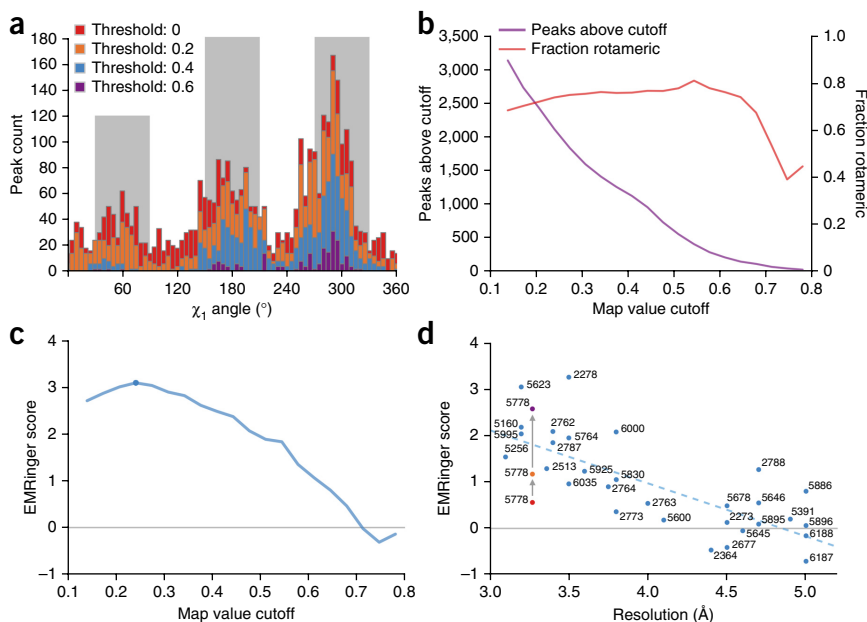

Figure 2 | EMRinger reveals statistical enrichment at rotameric χ_1 angles in high-resolution EM maps. (**a**) Histograms of EMRinger peaks for the T20S proteasome structure (EMDB 5623, PDB 3J9I) observed above multiple map value cutoffs. Rotameric regions of dihedral space are shown as gray bars. (**b**) The number of residues above the threshold (purple) and the fraction of those residues scored as rotameric by EMRinger (red), plotted against varying map value cutoffs. (**c**) EMRinger score plotted as a function of map value cutoff. It balances the sample size and the rotameric enrichment and is maximized at a cutoff of 0.242 for the proteasome structure (blue circle). (**d**) EMRinger scores for maps deposited in EMDB with atomic models, plotted against their resolution. A linear fit (R^2 = 0.549) is shown in blue dashes. For TrpV1, the deposited model (red, PDB 3J5P), the transmembrane domain of the deposited model (orange) and a model refined by Rosetta (purple, PDB 3J9J)[19] are all plotted.

Table 1 | Statistics before and after refinement

	Unrefined	Unrefined (transmembrane region)	Intermediate refinement	Final refinement
CC (3.27-Å cutoff)	0.676	0.726	0.715	0.728
CC (training map)	0.663	0.715	0.708	0.718
CC (testing map)	0.664	0.714	0.705	0.713
Integrated model-map FSC (15–3.4 Å)	0.473	0.553	0.513	0.526
All-atom clash score (MolProbity)	77.90	100.78	2.32	2.09
Modeled rotamer outliers (MolProbity)	26.6%	30.94%	0.35%	0%
EMRinger score	0.56	1.17	1.61	2.58

Cross-correlation, FSC_{mask}[19], MolProbity scores and EMRinger scores for the full, unrefined TrpV1 model (EMDB 5778, PDB 3J5P), the transmembrane domain of the unrefined model, an intermediate model during refinement of the transmembrane region and the final refined transmembrane region.
CC, cross-correlation.

as only the atoms modeled into the highest-resolution data remain (**Supplementary Fig. 1c** and **Supplementary Table 1**). We found that further rebuilding and refinement using Rosetta iterative local rebuilding[19] gradually improved the EMRinger score in most trials (**Supplementary Figs. 5** and **6a**). The best Rosetta trajectory improved the EMRinger score to 2.58, whereas the validation metrics for an independent reconstruction improved by a small margin (**Table 1** and **Supplementary Figs. 5** and **6b**). In contrast to existing measures, including real-space correlation or FSC[11], the EMRinger score was sensitive to features at lower map values, amplifying improvements in the model that show only a minor impact in the agreement-to-density term used by Rosetta refinement (**Table 1**). These results demonstrate how small corrections of backbone position along secondary structures, introduced through independently scored refinement procedures, can lead to improvements in the EMRinger score and the accuracy of the resulting model (**Supplementary Fig. 6c,d**).

Recent motion-corrected analyses have indicated that high-resolution information degrades as a function of total electron dose, probably as a result of radiation damage[20], and that the signal in the 5-Å shell degrades rapidly in the second half of data collection[21]. In addition to these global metrics, previous work has hypothesized that differential radiation damage causes negatively charged glutamate and aspartate residues to have weaker density than neutral but similarly shaped glutamine and asparagine residues[20,22,23]. To quantify the effect of radiation damage on the high-resolution features of the map and to address whether effects vary by residue type, we applied EMRinger to analyze dose-fractionated maps of the T20S proteasome. The overall EMRinger score degraded as a function of dose, with a sharp loss of signal beginning around the fifteenth frame, corresponding to a total dose of ~18 e⁻/Å² (**Fig. 3a**). Amino acids with charged side chains generally lost signal as a function of dose more quickly than average, whereas aromatic residues were much more resistant to degradation (**Fig. 3a**).

Most notably, negatively charged side chains lost signal much faster than positively charged side chains, with EMRinger score dropping to 0 by the map containing frames 6–10. Because a map comprising only noise (in the extreme of radiation damage) should result in a score of 0, differential damage is not sufficient to explain negative EMRinger scores observed in later frames. We observed that the initial map value peaks for some negatively charged residues inverted and became local minimums in later frames (**Fig. 3b,c**). This behavior is in contrast to the flattening effect, where a peak slowly degrades into noise, seen generally for other residue types (**Fig. 3d,e**). The inversion of the peak may result from the electron-scattering factors of negatively charged oxygen atoms, which are positive at high resolution but become negative at low resolution[24]. The net effect of the negative scattering behavior could therefore result in an enrichment of peaks
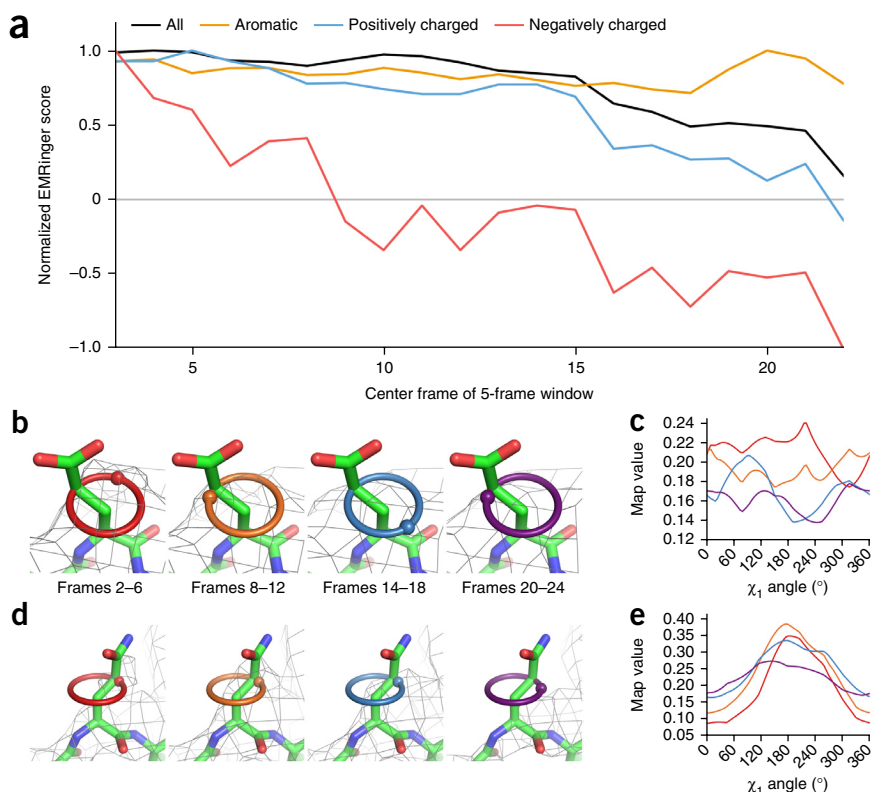
Figure 3 | Acidic residues are differentially altered by radiation damage. (**a**) Normalized EMRinger scores plotted for the T20S proteasome model (PDB 3J9I) against maps calculated from five frames of data. Scores are shown for the entire model (black), the aromatic residues (orange), positively charged residues (blue) and negatively charged residues (red). (**b**) Proteasome chain D residue Glu99 shown in density (isolevel 0.18) for maps generated from frames 2–6, 8–12, 14–18 and 20–24 (rings), with spheres showing local map value peaks. (**c**) EMRinger plots for Glu99 of chain D corresponding to the maps in **b**. Colors correspond to the frames shown in **b**. (**d**) Proteasome chain 1 residue Gln36 shown in density (isolevel 0.32) as in **b**. (**e**) EMRinger plots corresponding to the maps in **d**. Colors correspond to the frames shown in **d**.

at nonrotameric positions and, consequently, a negative EMRinger score after substantial radiation damage has accumulated.

Recent dramatic advances in cryo-EM have created new challenges in building, refining and validating atomic models. EMRinger extends and complements existing cryo-EM validation procedures in multiple ways. Whereas current methods[6] test conformational features independently of agreement with the map, EMRinger tests these features by querying the model and map together. The EMRinger score reports specifically on statistical signatures in high-resolution data. To validate the model-to-map correctness of atomic models from cryo-EM, refinement should result in EMRinger scores above 1.0 for well-refined structures with maps in the 3- to 4-Å range. EMRinger scores can be used in concert with cross-validation procedures[11] and other measures, such as gold-standard FSC-based resolution[4] and MolProbity statistics[6]. EMRinger scores can quantify improvements in the resolvability of atomic features owing to improvements to motion-correction algorithms, new data collection procedures that balance dose and radiation damage, and classification of particles representing distinct biochemical states[25].

Additionally, the high sensitivity of EMRinger suggests a natural direction for model building and refinement. At the resolutions commonly used for model building in EM, many closely related backbone conformations can fit the map density with nearly equal agreement. Given a nearly finalized backbone position, side chains with nonrotameric peaks can be adjusted to fix the Cγ atom in the peak density. Subsequently, the backbone conformation and closure to adjacent residues can be optimized to maintain a rotameric side chain conformation, similarly to the inverse rotamer approach used in some protein design applications[26]. Similar approaches to quantifying statistical signatures in weakly resolved data may also prove helpful for modeling of non–amino acid structures at lower resolutions, including glycans and nucleic acids[27,28].

METHODS

Methods and any associated references are available in the online version of the paper.

Accession codes. Protein Data Bank: Data have been deposited under accession numbers 3J9I (proteasome) and 3J9J (TrpV1).

Note: Any Supplementary Information and Source Data files are available in the online version of the paper.

Reprints and permissions information is available online at http://www.nature.com/reprints/index.html.

1. Liao, M., Cao, E., Julius, D. & Cheng, Y. *Curr. Opin. Struct. Biol.* **27**, 1–7 (2014).
2. Shi, Y. *Cell* **159**, 995–1014 (2014).
3. Wong, W. *et al. eLife* **3**, e03080 (2014).
4. Henderson, R. *et al. Structure* **20**, 205–214 (2012).
5. Scheres, S.H. & Chen, S. *Nat. Methods* **9**, 853–854 (2012).
6. Chen, V.B. *et al. Acta Crystallogr. D Biol. Crystallogr.* **66**, 12–21 (2010).
7. Ramachandran, G.N., Ramakrishnan, C. & Sasisekharan, V. *J. Mol. Biol.* **7**, 95–99 (1963).
8. Lovell, S.C., Word, J.M., Richardson, J.S. & Richardson, D.C. *Proteins* **40**, 389–408 (2000).
9. DiMaio, F., Zhang, J., Chiu, W. & Baker, D. *Protein Sci.* **22**, 865–868 (2013).
10. Amunts, A. *et al. Science* **343**, 1485–1489 (2014).
11. Falkner, B. & Schroder, G.F. *Proc. Natl. Acad. Sci. USA* **110**, 8930–8935 (2013).
12. Brown, A. *et al. Acta Crystallogr. D Biol. Crystallogr.* **71**, 136–153 (2015).
13. Lang, P.T., Holton, J.M., Fraser, J.S. & Alber, T. *Proc. Natl. Acad. Sci. USA* **111**, 237–242 (2014).
14. Lang, P.T. *et al. Protein Sci.* **19**, 1420–1431 (2010).
15. Zhou, A.Q., O'Hern, C.S. & Regan, L. *Proteins* **82**, 2574–2584 (2014).
16. Shapovalov, M.V. & Dunbrack, R.L. Jr. *Structure* **19**, 844–858 (2011).
17. Dunbrack, R.L. Jr. *Curr. Opin. Struct. Biol.* **12**, 431–440 (2002).
18. Liao, M., Cao, E., Julius, D. & Cheng, Y. *Nature* **504**, 107–112 (2013).
19. DiMaio, F. *et al. Nat. Methods* **12**, 361–365 (2015).
20. Allegretti, M., Mills, D.J., McMullan, G., Kuhlbrandt, W. & Vonck, J. *eLife* **3**, e01963 (2014).
21. Li, X. *et al. Nat. Methods* **10**, 584–590 (2013).
22. Bartesaghi, A., Matthies, D., Banerjee, S., Merk, A. & Subramaniam, S. *Proc. Natl. Acad. Sci. USA* **111**, 11709–11714 (2014).
23. Fioravanti, E., Vellieux, F.M., Amara, P., Madern, D. & Weik, M. *J. Synchrotron Radiat.* **14**, 84–91 (2007).
24. Mitsuoka, K. *et al. J. Mol. Biol.* **286**, 861–882 (1999).
25. Fernández, I.S. *et al. Science* **342**, 1240585 (2013).
26. Havranek, J.J. & Baker, D. *Protein Sci.* **18**, 1293–1305 (2009).
27. Cowtan, K. *IUCrJ* **1**, 387–392 (2014).
28. Terwilliger, T.C. *Acta Crystallogr. D Biol. Crystallogr.* **66**, 268–275 (2010).

ONLINE METHODS

Code availability. All scripts can be found at https://github.com/fraser-lab/EMRinger and can be run using Phenix/cctbx.python (version numbers greater than 1,894) or through an integrated graphical application (Phenix version numbers greater than 2,067). The scripts are also available in **Supplementary Software**.

Map values. We loaded CCP4-formatted maps using cctbx[29] and used the map voxel values without normalization, sharpening, filtering or other map manipulation. The wide range of normalization procedures used in constructing these maps explains the large differences in cutoff values used for different model-map pairs in our study. However, because EMRinger calculations are based on the relative values of a single map, we can compare EMRinger scores between maps without further normalization.

EMRinger map sampling and analysis. EMRinger, as implemented in the Phenix software package[29], is an extension of the Ringer protocol developed previously[13,14]. Ringer iteratively rotates side chain dihedral angles, interpolating the density at the terminal atom as it is rotated. We adapted EMRinger to work with real-space maps and to rotate the Cγ atom by increments of 5° around the χ1 dihedral angle (starting at 0° relative to the amide nitrogen). EMRinger calculates and records the map value from a potential map at the position of the Cγ atom at each increment using the eight-point interpolation function supplied by Phenix. From this scan, EMRinger records the peak map value and the angle at which it is achieved. These peak map values and angles are used for all further tools in the EMRinger package. EMRinger is available as phenix.emringer in Phenix (version dev-2016 or later). Real-space correlation coefficients were performed by the em_rscc.py script (https://github.com/fraser-lab/EMRinger and **Supplementary Software**).

Global EMRinger score calculation. We sampled all non-γ-branched, non-proline amino acids with a non-H γ atom, and measured the percent of map value peaks that are within at most 30° of 60°, 180° or 300° (which we classify as rotameric). With map values sampled every 5°, this leads to a total of 39 angle bins that are considered rotameric and 33 that are considered nonrotameric. The extra rotameric bins are due to cases that are exactly 30° away from the central angle of a bin, which are considered rotameric.

In order to separate the effects of peaks called from noise from peaks found in the density, we filtered peaks by a map value cutoff. If the map value of a peak is above this cutoff, it is interpreted as likely to be signal and therefore reporting correctly on the backbone position. Map values below this cutoff are discarded. Rather than relying on a user-selected map value cutoff, EMRinger chooses a range of 20 cutoffs, sampling linearly from the average map value across all scanned residues to the maximum map value measured across all scanned residues, and calculates statistics about the distribution for each possible cutoff.

To determine the significance of this distribution, we calculated a Z-score based on a normal approximation to the binomial distribution (equation (1)).

$$Z\text{-score}_{threshold} = \frac{\text{Number rotameric} - \frac{39}{72} \times \text{Number above threshold}}{\sqrt{\frac{39}{72}\left(1 - \frac{39}{72}\right) \times \text{Number above threshold}}} \quad (1)$$

Number rotameric is the number of peaks above the cutoff that had rotameric chi angles, and number above cutoff is the total number of peaks above the cutoff. 39/72 is the distribution for the null hypothesis as predicted by the binomial distribution for 72 bins with 39 rotameric choices.

To compare Z-scores between models of different structures, the Z-score is rescaled to the EMRinger score to account for the total number of amino acids in the model (equation (2)).

$$\text{EMRinger score}_{threshold} = \frac{10 \times Z\text{-score}_{threshold}}{\sqrt{\text{Model length}}} \quad (2)$$

Z-score is the output of equation (1). Model length is the total number of amino acids in the model that were scanned by EMRinger regardless of cutoff: all non–γ-branched, non-proline amino acids with a modeled non-H γ atom.

EMRinger repeats these calculations across the range of map value cutoffs. The highest score calculated across this range of cutoffs is returned as the EMRinger score for the model-map pair. Because of this multiple testing and the correction to account for varying model length, the final EMRinger score should not be used as a Z-score for statistical purposes.

EMRinger score does not change when the model and map are multiplied (for example, in the case of a polymer with high symmetry), so that the score is definitive and no questions arise of how many monomers should be included in the analysis. An EMRinger score of 1.0 sets an initial quality goal for a model refined against a map in the 3.2–3.5 Å range, whereas very high-quality models at high resolution generate scores above 2.0. Maps that are highly variable in resolution may have lower EMRinger scores unless poorly resolved regions of the map are masked out and excluded from the model. Calculation of the EMRinger score is performed by the emringer_score.py script (https://github.com/fraser-lab/EMRinger and **Supplementary Software**).

Rolling window EMRinger analysis. In order to quantify the local contributions to the EMRinger score, we perform EMRinger analysis on rolling 21-residue windows along the primary sequence of proteins. For each window, we calculated the fraction of residues whose peaks were rotameric. These values were plotted as a function of the window position and compared between different models of a protein to distinguish regions of improved model quality. Rolling window EMRinger analysis is performed by the emringer_rolling.py script (https://github.com/fraser-lab/EMRinger and **Supplementary Software**).

Refinement of TrpV1 with Rosetta iterative local rebuilding.
Refinement of TrpV1 used an iterative local rebuilding procedure to improve local backbone geometry as well as fit to the experimental density data[19]. Refinement began with the deposited PDB structure of TrpV1 (PDB 3J5P). The model was trimmed to the transmembrane region (residues 381–695), and bond angles and bond lengths were given ideal geometry. During local rebuilding, five cycles of backbone rebuilding were run; in each cycle, regions with poor fit to density or poor local geometry were automatically identified, and rebuilding focused on these regions. Each rebuilding cycle was followed by side chain rotamer optimization and all-atom refinement with a physically realistic force field. Following this protocol, 1,000 independent trajectories were run, and the final model was selected by filtering on two criteria: first, the 800 most nonphysical models were eliminated by assessing each model against the Rosetta all-atom force field; second, fit-to-density was used to rank models and select the best model from these 200.

Table statistics. The cross-correlation was calculated using Chimera's 'fit in map' tool across all contours and using a resolution cutoff for the calculated map. The integrated FSC was calculated between the model and an independent reconstruction over a masked region covering the protein only. The mask was truncated at 6-Å resolution, and we report the integrated FSC_{mask} over high-resolution shells only (15 to ~3.4 Å). MolProbity statistics were calculated using the validate tool in Phenix nightly build 1894.

Radiation damage analysis. To identify the degradation of map signal with radiation damage, we used EMRinger with a single model across multiple dose-fractionated maps. Individual reconstructions were calculated on the basis of each of the 24 frames of data collected using the alignments generated from the full reconstruction in Frealign[21]. Five-frame averages were generated by voxel-by-voxel averaging between each of the five frames using the CCP4 'mapmask' tool. For each five-frame averaged dose-fractionated map, the EMRinger score is calculated for the full model. We additionally calculated EMRinger scores for subsets of the model comprising only the aromatic, positively charged or negatively charged residues to compare the differential radiation damage effects for different amino acid classes.

Radiation damage can lead to a negative scattering contribution near the true (rotameric) position in subsequent maps. Because the rotameric peak of the original map can therefore be lowered below the baseline, EMRinger will then identify a new peak at a different local maximum in the damaged map. This new local maximum is more likely to occur at nonrotameric angles because the original rotameric angle is now suppressed by negative scattering contributions in the damaged map. The results of the EMRinger analysis on dose-fractionated data suggest that reconstructions based on different doses may be required to maximize the resolvability of different sets of side chains, just as different degrees of sharpening are commonly used now during model building.

Residue-specific sampling was performed by the emringer_residue.py script (https://github.com/fraser-lab/EMRinger and **Supplementary Software**).

Grid spacing adjustment. In order to change the grid spacing of maps to test the effect of grid spacing on EMRinger scores, real-space maps were first Fourier transformed to structure factors using phenix.map_to_structure_factors[29]. The maps were then transformed back into real space with specified grid spacing using phenix.mtz2map with variations in grid_resolution_factor[29] to vary the grid spacing without affecting the resolution.

29. Adams, P.D. *et al. Acta Crystallogr. D Biol. Crystallogr.* **66**, 213–221 (2010).